Supporting material for "Bond graph modelling of the cardiac action potential: Implications for drift and non-unique steady states"

Michael Pan[1], Peter J. Gawthrop[1], Kenneth Tran[2], Joseph Cursons[3,4], Edmund J. Crampin[1,5,6,*]

[1]Systems Biology Laboratory, School of Mathematics and Statistics, and Department of Biomedical Engineering, Melbourne School of Engineering, University of Melbourne, Parkville, Victoria 3010, Australia

[2]Auckland Bioengineering Institute, University of Auckland

[3]Bioinformatics Division, Walter and Eliza Hall Institute of Medical Research, Parkville, Victoria 3052, Australia

[4]Department of Medical Biology, School of Medicine, University of Melbourne, Parkville, Victoria 3010, Australia

[5]ARC Centre of Excellence in Convergent Bio-Nano Science and Technology, Melbourne School of Engineering, University of Melbourne, Parkville, Victoria 3010, Australia

[6]School of Medicine, University of Melbourne, Parkville, Victoria 3010, Australia

*Corresponding author. Email: edmund.crampin@unimelb.edu.au

A Fitting ion channel parameters

A.1 I-V equations

A variety of methods were used to fit permeability constants P for the GHK equations used for the bond graph model. For some channels, P could be determined algebraically (such as the Na^+ and L-type Ca^{2+} channels). For others, optimisation was required to reduce error between the fitted I-V curve $I_{\mathrm{GHK}}(V)$ (see Eq. 2.14) and Luo-Rudy I-V curve $I_{\mathrm{LR}}(V)$. In these cases, fitting was weighted towards $-90\ \mathrm{mV} \leq V \leq -30\ \mathrm{mV}$ for I_{K1}, $-20\ \mathrm{mV} \leq V < 30\ \mathrm{mV}$ for I_{K}, and $0\ \mathrm{mV} \leq V \leq 60\ \mathrm{mV}$ for I_{Kp}. These regions were chosen based on when those channels activated. Where applicable, the optimisation problem was carried out by using particle swarm optimisation [1] followed by a local nonlinear optimiser. The permeabilities from fitting I-V curves are summarised in Table S1.

Table S1: Permeabilities of the GHK equations used for the bond graph model.

Permeability	Value (pL/s)
P_{Na}	9.0602
P_{K1}	1.1200
P_{K}	0.2299
P_{Kp}	0.0136
P_{CaL}	28.2471
P_{KL}	0.0222

A.1.1 Sodium current

The permeability was chosen so match the linear equation at the negative of the Nernst potential [2]:

$$P_{\mathrm{Na}} = \frac{2\bar{G}_{\mathrm{Na}}(1 - \exp\left[FE_{\mathrm{Na}}/(RT)\right])}{[\mathrm{Na}_{\mathrm{i}}^+] - [\mathrm{Na}_{\mathrm{e}}^+]\exp\left[FE_{\mathrm{Na}}/(RT)\right]}\frac{RT}{F^2} \tag{S1}$$

where

$$E_{\mathrm{Na}} = \frac{RT}{F}\ln\left(\frac{[\mathrm{Na}_{\mathrm{e}}^+]}{[\mathrm{Na}_{\mathrm{i}}^+]}\right) \tag{S2}$$

$$\bar{G}_{\mathrm{Na}} = 2.45\ \mu\mathrm{A/mV} \tag{S3}$$

A.1.2 Time-independent K^+ current

$$P_{\mathrm{K1}} = \arg\min_{P}\left\{\sum_{V=-90}^{-30}\left[I_{\mathrm{K1,LR}}(V) - I_{\mathrm{K1,GHK}}(V,P)\right]^2\right\} \tag{S4}$$

$$I_{\mathrm{K1,LR}}(V) = \bar{G}_{\mathrm{K1}}(V - E_{\mathrm{K}}) \tag{S5}$$

$$\bar{G}_{\mathrm{K1}} = 1.1505 \times 10^{-4}\ \mu\mathrm{A/mV} \tag{S6}$$

$$E_{\mathrm{K}} = \frac{RT}{F}\ln\left(\frac{[\mathrm{K}_{\mathrm{e}}^+]}{[\mathrm{K}_{\mathrm{i}}^+]}\right) \tag{S7}$$

$$\tag{S8}$$

A.1.3 Time-dependent K^+ current

$$P_{\mathrm{K}} = \arg\min_{P} \left\{ \sum_{V=-20}^{29} \left[I_{\mathrm{K,LR}}(V) - I_{\mathrm{K,GHK}}(V,P) \right]^2 \right\} \tag{S9}$$

$$I_{\mathrm{K,LR}}(V) = \bar{G}_{\mathrm{K}}(V - E_{\mathrm{K,LR}}) \tag{S10}$$

$$\bar{G}_{\mathrm{K}} = 4.3259 \times 10^{-5}\ \mu\mathrm{A/mV} \tag{S11}$$

$$E_{\mathrm{K,LR}} = \frac{RT}{F} \ln\left(\frac{[\mathrm{K_e^+}] + P_{\mathrm{Na,K}}[\mathrm{Na_e^+}]}{[\mathrm{K_i^+}] + P_{\mathrm{Na,K}}[\mathrm{Na_i^+}]} \right) \tag{S12}$$

$$P_{\mathrm{Na,K}} = 0.01833 \tag{S13}$$

Note that the Luo and Rudy I-V relationship for the time-dependent K^+ current (Eq. S10) is thermodynamically inconsistent because $E_{\mathrm{K,LR}}$ is not the Nernst potential defined in Eq. S7. As a result, nonzero currents can result at the Nernst potential, where the current should be zero from thermodynamic constraints. Despite this thermodynamic inconsistency, it is possible to define $I_{\mathrm{K,GHK}}(V)$, a thermodynamically consistent approximation to the I-V curve in Luo and Rudy.

A.1.4 Plateau K^+ current

$$P_{\mathrm{Kp}} = \arg\min_{P} \left\{ \sum_{V=0}^{60} \left[I_{\mathrm{Kp,LR}}(V) - I_{\mathrm{Kp,GHK}}(V,P) \right]^2 \right\} \tag{S14}$$

$$I_{\mathrm{Kp,LR}}(V) = \bar{G}_{\mathrm{Kp}}(V - E_{\mathrm{K}}) \tag{S15}$$

$$\bar{G}_{\mathrm{Kp}} = 2.8072 \times 10^{-6}\ \mu\mathrm{A/mV} \tag{S16}$$

$$\tag{S17}$$

E_{K} same as for the time-independent K^+ current.

A.1.5 L-type Ca^{2+} channel

For the L-type Ca^{2+} channel, Luo and Rudy [3] use the I-V equation

$$I_{\mathrm{Ca}} = P_{\mathrm{Ca}} \frac{z^2F^2V}{RT} \frac{\gamma_{\mathrm{Cai}}[\mathrm{Ca_i^{2+}}]\exp(zFV/RT) - \gamma_{\mathrm{Cae}}[\mathrm{Ca_e^{2+}}]}{\exp(zFV/RT) - 1} \tag{S18}$$

which resembles the GHK equation, but allows thermodynamic laws to be broken through the use of different partitioning factors γ_{si} and γ_{so}. In the case of the Ca^{2+} component of the current, this was resolved by setting both factors to the value of γ_{Cao}, with little effect on the I-V curve. Thus the permeabilities of the GHK equations are calculated as follows:

$$P_{\mathrm{CaL}} = P_{\mathrm{CaL,LR}}\gamma_{\mathrm{Cae}} \tag{S19}$$

$$P_{\mathrm{KL}} = P_{\mathrm{KL,LR}}\gamma_{\mathrm{Ke}} = P_{\mathrm{KL,LR}}\gamma_{\mathrm{Ki}} \tag{S20}$$

where

$$P_{\mathrm{CaL,LR}} = 8.2836 \times 10^{-8}\ \mathrm{cm^3/s} \tag{S21}$$

$$P_{\mathrm{KL,LR}} = 2.9606 \times 10^{-11}\ \mathrm{cm^3/s} \tag{S22}$$

$$\gamma_{\mathrm{Cae}} = 0.341 \tag{S23}$$

$$\gamma_{\mathrm{Ke}} = \gamma_{\mathrm{Ki}} = 0.75 \tag{S24}$$

A.2 Gating transition parameters

The parameters derived for gate transition are summarised in Table S2, with further detail described below.

Table S2: Gate transition parameters.

Gate	α_0 (s^{-1})	z_f	β_0 (s^{-1})	z_r
m	12516.4361	0.4954	79.9996	−2.4284
h	0.00033539	−4.1892	799.9028	1.2995
j	0.00013079	−4.0381	422.7582	1.4281
K1	1127.3395	0.0336	13544806.3586	3.1153
X	2.2317	0.5192	0.5750	−0.7317
Xi	995.8931	0	172.6026	0.8322
Kp	999.8464	0	3497.4018	−4.4669
d	486.7619	2.1404	98.0239	−2.1404
f	See § B.3			

A.2.1 m, h, j, K1 and X-gates

A vector quantity $\mathbf{p} = (\alpha_0, z_f, \beta_0, z_r)$ was optimised based on the quality of fits to the transition parameters, steady-state open probability and time constant in the range -120 mV $\leq V \leq$ 60 mV:

$$\mathbf{p}_g = \arg\min \left\{ \sum_{V=-120}^{60} a(V) \Big(a_\alpha \left[\alpha_{g,\mathrm{LR}}(V) - \alpha_g(V,\mathbf{p})\right]^2 + a_\beta \left[\beta_{g,\mathrm{LR}}(V) - \beta_g(V,\mathbf{p})\right]^2 + a_{\mathrm{gss}} \left[g_{ss,\mathrm{LR}}(V) - g_{\mathrm{ss}}(V,\mathbf{p})\right]^2 + a_\tau \left[\tau_{g,\mathrm{LR}}(V) - \tau_g(V,\mathbf{p})\right]^2 \Big) \right\} \tag{S25}$$

where g is replaced with m, h, j, K1 or X depending on the gate. $a(V) = 1$ and $a_\alpha = a_\beta = a_{\mathrm{gss}} = a_\tau = 1$ for the m, h and j gates. For the K1 gate, $a(V) = 1$, $a_\alpha = a_\beta = 0$, $a_\tau = 1$ and $a_{\mathrm{gss}} = 1000$. For the X gate,

$$a_{\mathrm{gss}} = 100, \qquad a(V) = \begin{cases} 1, & V < 0 \text{ mV} \\ 25, & V \geq 0 \text{ mV} \end{cases} \tag{S26}$$

The parameters α_g and β_g have unit ms^{-1} and τ_g has unit ms. Optimisation was carried out using particle swarm optimisation followed by a local optimiser.

A.2.2 Xi-gate

To give a perfect fit for $\mathrm{Xi}_{\mathrm{ss}}$,

$$\alpha_0 = K_{\mathrm{Xi}} \tag{S27}$$

$$\beta_0 = K_{\mathrm{Xi}} e^{56.26/32.1} \tag{S28}$$

$$z_f = 0 \tag{S29}$$

$$z_r = \frac{RT}{F} \frac{1000\mathrm{mV/V}}{32.1\mathrm{mV}} = 0.8322 \tag{S30}$$

To achieve a time constant of less than 1ms in the range -120 mV $\leq V \leq 60$ mV, we chose

$$K_{\mathrm{Xi}} = 0.9959 \tag{S31}$$

A.2.3 Kp-gate

To give a perfect fit for $\mathrm{Kp}_{\mathrm{ss}}$,

$$\alpha_0 = K_{\mathrm{Kp}} \tag{S32}$$
$$\beta_0 = K_{\mathrm{Kp}} e^{7.488/5.98} \tag{S33}$$
$$z_f = 0 \tag{S34}$$
$$z_r = \frac{RT}{F}\frac{1000\mathrm{mV/V}}{5.98\mathrm{mV}} = -4.4669 \tag{S35}$$

To achieve a time constant of less than 1ms in the range -120 mV $\leq V \leq 60$ mV, we chose

$$K_{\mathrm{Kp}} = 0.9998 \tag{S36}$$

A.2.4 d-gate

To give a perfect fit for d_{ss},

$$\alpha_0 = K_d e^{10/12.48} \tag{S37}$$
$$\beta_0 = K_d e^{-10/12.48} \tag{S38}$$
$$z_f = \frac{RT}{F}\frac{1000\mathrm{mV/V}}{12.48\mathrm{mV}} = 2.1404 \tag{S39}$$
$$z_r = -\frac{RT}{F}\frac{1000\mathrm{mV/V}}{12.48\mathrm{mV}} = -2.1404 \tag{S40}$$

K_d was chosen to match the peak time constant because that is where changes would be most likely to make a difference given that the time constant is small:

$$K_d = 0.2184 \tag{S41}$$

B Channel-specific modelling issues

B.1 K^+ regulation of K^+ currents

For the K and K1 channels, Luo and Rudy [3] describe a dependence of the permeability on the square root of extracellular K^+ concentration:

$$G = G_{\mathrm{ch}}\sqrt{[\mathrm{K}^+]_{\mathrm{e}}} \tag{S42}$$

where G_{ch} is a constant value that differs between the two channels. This was incorporated by assigning an additional extracellular K^+ stoichiometry of 0.5 to both sides of the ion transport reaction, which results in an ion channel current of

$$v = \kappa(V)\left(K_{Ke}^{0.5}x_{Ke}^{0.5}K_{Ki}x_{Ki}e^{zFV/RT} - K_{Ke}^{1.5}x_{Ke}^{1.5}\right) \tag{S43}$$
$$= \kappa(V)\sqrt{K_{Ke}x_{Ke}}\left(K_{Ki}x_{Ki}e^{zFV/RT} - K_{Ke}x_{Ke}\right) \tag{S44}$$

B.2 Ca^{2+} inactivation of L-type Ca^{2+} current

Luo and Rudy [3] describe a mechanism whereby the L-type Ca^{2+} channel is inactivated by intracellular Ca^{2+}, using the function:

$$f_{\mathrm{Ca}} = \frac{1}{1 + ([\mathrm{Ca}_{\mathrm{i}}^{2+}]/K_{m,\mathrm{Ca}})^2} \tag{S45}$$

This mechanism was incorporated into the bond graph framework through the reaction:

$$A + 2\mathrm{Ca_i} \rightleftharpoons I \tag{S46}$$

with a dissociation constant equal to $K_{m,\mathrm{Ca}}^2$. It can be shown that at equilibrium:

$$\frac{x_A}{x_A + x_I} = \frac{1}{1 + ([\mathrm{Ca_i^{2+}}]/K_{m,\mathrm{Ca}})^2} = f_{\mathrm{Ca}} \tag{S47}$$

Therefore Ca^{2+} inactivation was incorporated by applying the reaction in Eq. S46 to each of the states that result from independent d and f gating, using kinetic constants that were sufficiently high to approximate rapid equilibrium.

B.3 f-gate of the L-type Ca^{2+} channel

Luo and Rudy use the equations from Rasmusson *et al.* [4] for their L-type Ca^{2+} channel f-gate, resulting in U-shaped functions for both the steady-state open probability f_{ss} and time constant τ_f. Using the exponential dependence in Eq. 2.21, f_{ss} must have a monotonic and sigmoidal shape, and τ_f must either be bell-shaped or monotonic. As neither the f_{ss} nor τ_f could be made U-shaped with the current formulation, we used an alternative mechanism to describe the f-gate. We observed that the f-gate activated at both negative and positive voltages, and that the minima of f_{ss}, and τ_f of the Rasmusson equations appeared to coincide. We modelled the gate using the reaction network $O_1 \underset{\alpha_1}{\overset{\beta_1}{\rightleftharpoons}} C \underset{\beta_2}{\overset{\alpha_2}{\rightleftharpoons}} O_2 \underset{k_3^+}{\overset{k_3^-}{\rightleftharpoons}} O_1$ with the final reaction assumed to be at quasi-equilibrium. The rationale behind using this three-state model was that: (a) there were two open states, one that activated at negative voltages and one that activated at positive voltages, and; (b) the inactivation parameters could be chosen such that the gate inactivated faster than it activated. The initial spike in membrane potential during an action potential implies that the open probability is unable to change, thus we used a reaction in rapid equilibrium to convert between the two open states; without this, the gate would need to pass the closed states to move between the open states.

Similar to the transition parameters in other gates an exponential dependence on voltage was assumed. Since the mechanism involves a biochemical cycle, a detailed balance constraint was used to determine parameters for the third reaction between the two open states:

$$\frac{k_3^+(V)}{k_3^-(V)} = \frac{\beta_1(V)\alpha_2(V)}{\alpha_1(V)\beta_2(V)} \tag{S48}$$

The following information was used to parameterise the f-gate:

1. The difference between the steady-state open probabilities in the Luo-Rudy model (f_{ss}) and bond graph model ($f_{\mathrm{ss,BG}}$) over the range -90 mV $\leq V \leq 50$ mV. The open probability of the bond graph formulation was calculated by rapid equilibrium arguments [5]:

$$f_{\mathrm{ss,BG}} = \frac{\alpha_1/\beta_1 + \alpha_2/\beta_2}{1 + \alpha_1/\beta_1 + \alpha_2/\beta_2} \tag{S49}$$

   Differences were taken between the natural logarithms of each of the open probabilities prior to calculating differences to better match lower values.

2. Simulations of the f-gate were run with the voltage held constant. The open probabilities over time were compared to solutions obtained from the Luo-Rudy formulation of the f-gate. The conditions for the simulations are summarised in Table S3. For computational efficiency, the third reaction was neglected for the bond graph simulations. All simulations involve either activation/inactiation processes involving one of the open states. It was assumed that very little of the of the other open state would become open.

Table S3: Summary of conditions used to simulate f-gate for fitting parameters. o_1, c and o_2 represent the proportion of the three states representing the inactivation process.

#	Voltage (mV)	Initial conditions	Description
1	−80	$o_1 = 0$, $c = 1$, $o_2 = 0$	Activation at −80 mV
2	−40	$o_1 = 1$, $c = 0$, $o_2 = 0$	Inactivation at −40 mV
3	−40	$o_1 = 0$, $c = 1$, $o_2 = 0$	Activation at −40 mV
4	0	$o_1 = 1$, $c = 0$, $o_2 = 0$	Inactivation at 0 mV from O_1
5	0	$o_1 = 0$, $c = 0$, $o_2 = 1$	Inactivation at 0 mV from O_2
6	40	$o_1 = 0$, $c = 0$, $o_2 = 1$	Inactivation at 40 mV

The transition rates for the f-gate are

$$\alpha_1(V) = \alpha_{0,1} \exp\left(\frac{z_{f,1}FV}{RT}\right) \tag{S50}$$

$$\beta_1(V) = \beta_{0,1} \exp\left(\frac{z_{r,1}FV}{RT}\right) \tag{S51}$$

$$\alpha_2(V) = \alpha_{0,2} \exp\left(\frac{z_{f,2}FV}{RT}\right) \tag{S52}$$

$$\beta_2(V) = \beta_{0,2} \exp\left(\frac{z_{r,2}FV}{RT}\right) \tag{S53}$$

$$k_3^+(V) = r_3 K_{3,0} \exp\left(\frac{z_{f,3}FV}{RT}\right) \tag{S54}$$

$$k_3^- = r_3 \tag{S55}$$

with the constants

$$\alpha_{0,1} = 0.8140 \text{ s}^{-1}, \qquad z_{f,1} = -1.1669 \tag{S56}$$

$$\beta_{0,1} = 36.1898 \text{ s}^{-1}, \qquad z_{r,1} = 1.6709 \tag{S57}$$

$$\alpha_{0,2} = 1.6369 \text{ s}^{-1}, \qquad z_{f,2} = 0.7312 \tag{S58}$$

$$\beta_{0,2} = 35.5248 \text{ s}^{-1}, \qquad z_{r,2} = -0.5150 \tag{S59}$$

$$r_3 = 10000 \text{ s}^{-1}, \qquad K_{3,0} = 2.0485 \tag{S60}$$

$$z_{f,3} = z_{r,1} + z_{f,2} - z_{f,1} - z_{r,2} = 4.0839 \tag{S61}$$

The three-state scheme in the bond graph framework produced a similar curve for f_{ss} to the f-gate of the Luo-Rudy model (Figure S1A). Since there is no direct time constant for our three-state model we compared the dynamic behaviour of the f-gates by simulating to an action potential-like voltage waveform (Figure S1B). During the depolarised phase of the action potential where the f-gate steadily inactivates, the bond graph model provides a very good fit to the Luo and Rudy model (Figure S1C). In the resting phase the bond graph model reactivates faster, but still provides a reasonable fit.

C Ion transporters

C.1 Na^+/K^+ ATPase

We used the 15-state bond graph model described in Pan *et al.* [6], with a pump density of 4625 µm^{-2} (0.1178 fmol per cell).

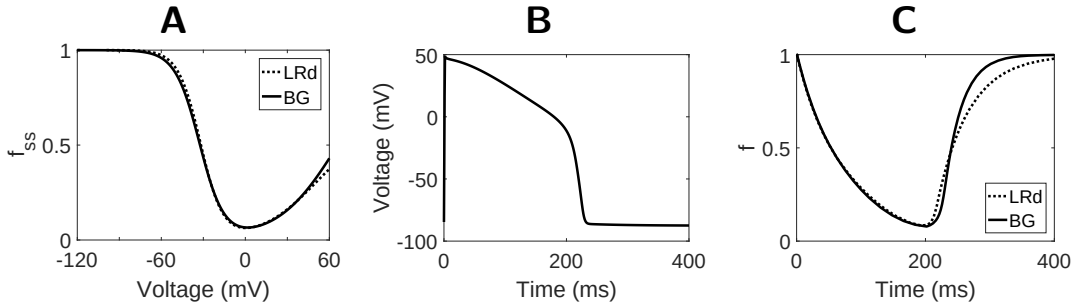

Figure S1: Fitting the f-gate of the L-type Ca^{2+} channel. (A) The steady-state open probability of the f-gate, calculated by adding the proportion of the two open states. **(B)** The action potential waveform used to compare the behaviour of the Luo and Rudy (LRd) and bond graph (BG) formulations of the f-gate. This was obtained by simulating the Luo-Rudy model with the ion channels used in this study, and holding the ion concentrations constant. **(C)** The response of the f-gates to the voltage signal in B.

C.2 Na^+-Ca^{2+} exchanger

The NCX was modelled using the bond graph shown in Figure S2. The reaction scheme was based on the ping-pong mechanism proposed in Giladi *et al.* [7], with reactions r1, r2, r4 and r5 modelled by fast rate constants to approximate rapid equilibrium. We assigned voltage dependence to translocation of Na^+, based on experimental findings from Hilgemann *et al.* [8].

Using similar methods to Luo and Rudy [3], the NCX model was fitted to the following data, assuming steady-state operation:

1. Dependence of cycling rate on extracellular Na^+ and voltage, from Kimura *et al.* [9].
2. Dependence of cycling rate on extracellular Ca^{2+}, from Kimura *et al.* [9]. Data obtained at $V < -50$ mV and $[Ca^{2+}]_e = 1$ mM were excluded from the fitting process.
3. To incorporate behaviour for another intracellular Ca^{2+} concentration, data from Beuckelmann and Wier [10] were used. Data obtained at $V < -120$ mV were excluded from the fitting process.

Parameters of the model were identified using particle swarm optimisation followed by a local optimiser, and a comparison between the model and data is shown in Figure S3. The model closely matched the data describing extracellular Na^+ dependence (Figure S3A). Reasonable fits were obtained for the other data, although there was some discrepancy at negative voltages in Figure S3B. There was some difference between the model and data from Beuckelmann and Wier [10] (Figure S3C), although this appears to have resulted from differences in the equilibrium point.

The cycling velocity was normalised to 700 s^{-1} at the normalisation point of Figure S3A to approximately match experimental currents at a membrane capacitance of 200 pF and 300 sites per μm^{-2}. To ensure that the exchanger current had a similar magnitude to that of Luo and Rudy [3], we used a site density of 170 μm^{-2} (0.0043 fmol per cell) in our cardiac action potential model.

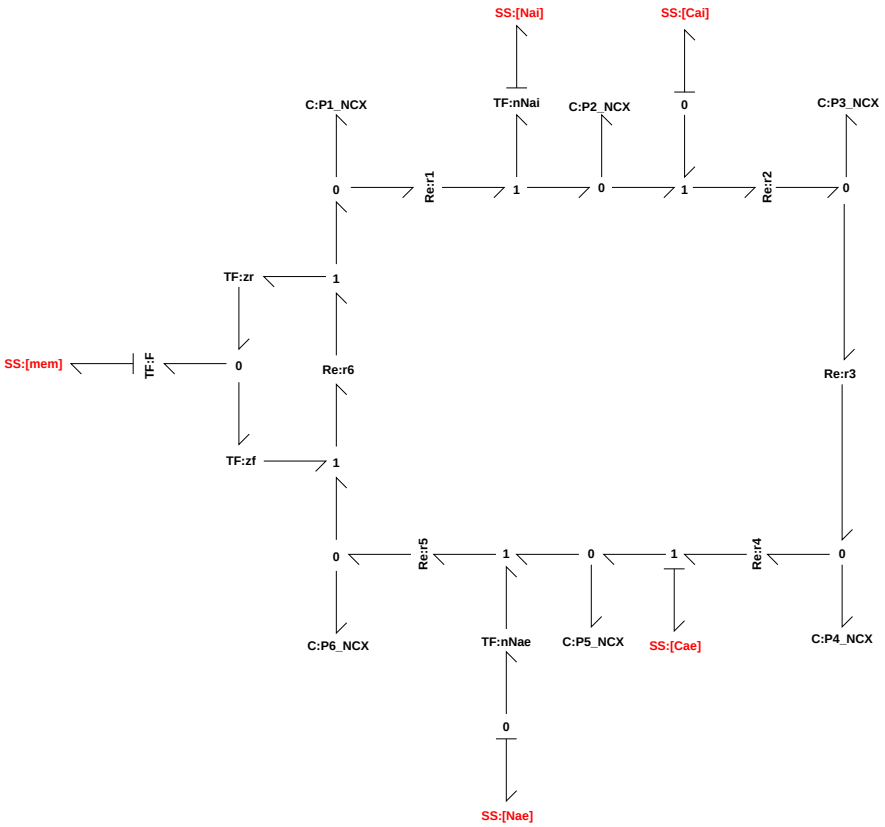

Figure S2: The bond graph model of NCX.

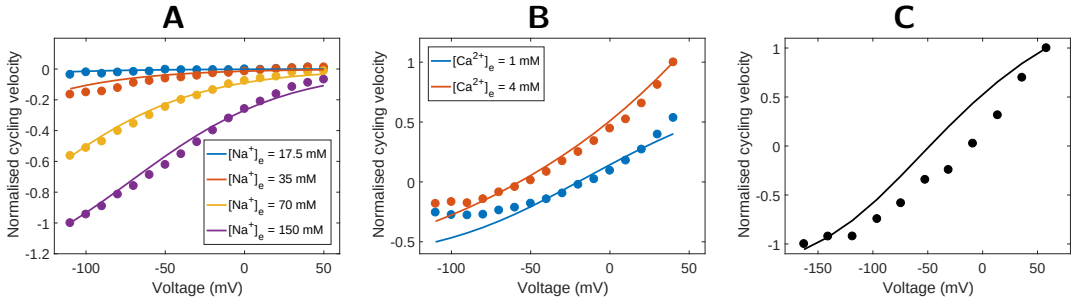

Figure S3: Fit of NCX model to data. **(A)** Comparison of model to Fig. 8B of Kimura *et al.* [9]. Fluxes were normalised to the value at $[Na^+]_e = 140$ mM and $V = -110$ mV. $[Na^+]_i = 0$ mM, $[Ca^{2+}]_e = 1$ mM, $[Ca^{2+}]_i = 430$ nM. **(B)** Comparison of model to Fig. 9A of Kimura *et al.* [9]. Fluxes were normalised to the value at $[Ca^{2+}]_e = 4$ mM and $V = 40$ mV. $[Na^+]_e = 140$ mM, $[Na^+]_i = 10$ mM, $[Ca^{2+}]_i = 172$ nM. **(C)** Comparison of model to Fig. 6B of Beuckelmann and Wier [10]. Fluxes were normalised to the value at $V = 60$ mV. $[Na^+]_e = 135$ mM, $[Na^+]_i = 15$ mM, $[Ca^{2+}]_e = 2$ mM, $[Ca^{2+}]_i = 450$ nM.

D Ca^{2+} buffering

The model of Ca^{2+} buffering was based on the equations described in Luo and Rudy [3]. These equations represent the reactions

$$\mathrm{TRPN} + \mathrm{Ca}_\mathrm{i}^{2+} \rightleftharpoons \mathrm{TRPNCa} \tag{S62}$$

$$\mathrm{CMDN} + \mathrm{Ca}_\mathrm{i}^{2+} \rightleftharpoons \mathrm{CMDNCa} \tag{S63}$$

with the dissociation constants $K_{\mathrm{d,TRPN}} = 0.5$ µM and $K_{\mathrm{d,CMDN}} = 2.38$ µM. The total concentrations of each buffer were 70 µM for troponin and 50 µM for calmodulin. The reactions were modelled using sufficiently fast kinetic constants to approximate rapid equilibrium, and the amount of Ca^{2+} bound to each buffer was initialised to the value at equilibrium for the initial intracellular Ca^{2+} concentration of 0.12 µM.

E Bond graph parameters

E.1 Calculating bond graph parameters

Bond graph parameters were found by using an extension of the method presented in Gawthrop *et al.* [11]. The kinetic parameters and bond graph parameters can be related through the matrix equation

$$\mathbf{Ln}(\mathbf{k}) = \mathbf{M}\mathbf{Ln}(\mathbf{W}\boldsymbol{\lambda}) \tag{S64}$$

where

$$\mathbf{k} = \begin{bmatrix} k^+ \\ k^- \end{bmatrix}, \quad \mathbf{M} = \left[\begin{array}{c|c} I_{n_r \times n_r} & N^{f\,T} \\ \hline I_{n_r \times n_r} & N^{r\,T} \end{array}\right], \quad \boldsymbol{\lambda} = \begin{bmatrix} \kappa \\ K \end{bmatrix} \tag{S65}$$

k^+ is a column vector consisting of the forward kinetic constants, k^- is a column vector consisting of the reverse kinetic constants, N^f and N^r are the forward and reverse stoichiometric matrices respectively, κ is a column vector of bond graph reaction rate constants, and K is column vector of thermodynamic constants. To account for the volumes of each compartment, $\mathbf{W}$ is a diagonal matrix where the i-th diagonal element is the volume corresponding to i-th bond graph component (either a reaction or species). Depending on compartment, the elements corresponding to each ion were set to either the intracellular volume of $W_i = 38$ pL or the extracellular volume of $W_e = 5.182$ pL. All other diagonal entries were set to 1. Assuming that detailed balance constraints are satisfied, a solution to Eq. S64 is

$$\boldsymbol{\lambda_0} = \mathbf{W}^{-1}\mathbf{Exp}(\mathbf{M}^\dagger\mathbf{Ln}(\mathbf{k})) \tag{S66}$$

where $\mathbf{M}^\dagger$ is the pseudo-inverse of $\mathbf{M}$. All parameters were identified using $T = 310$ K.

For reactions involved in ion transport that use the GHK equation, both the forward and reverse rate constants were set to P/x_{ch}, where P is the permeability constant found by fitting to Eq. 2.14, and x_{ch} is the total number of channels. The values of x_{ch} used for each channel are given in Table S4. Since the bond graph paramters of the NCX model were fitted to kinetic data, the bond graph paramters were converted back to kinetic paramters [11] to parameterise the action potential model.

Table S4: Amounts of each ion channel per cell. A geometric area of 0.767×10^{-4} cm^2 was used to convert between channel density and channels per cell (x_{ch}).
*Quantity cited from reference.

Ion channel	Channel density (µm^{-2})	Channels per cell	Reference
Na	16*	122720	[12]
K1	1.8*	4261	[13]
K	0.7*	5369	[14]
Kp	0.095	725*	[15]
LCC	6.5	50000*	[16]

F Charge conserved moiety

In Table 1 of the main text, Σ is defined as

$$\begin{aligned}\Sigma = &+ 3.0818\text{C}_{\text{K1}} - 1.6697\text{S}_{00,\text{K}} - 0.4188\text{S}_{10,\text{K}} + 0.8322\text{S}_{20,\text{K}} - 2.5019\text{S}_{01,\text{K}} \\ &- 1.2509\text{S}_{11,\text{K}} - 4.4669\text{C}_{\text{Kp}} + 2.1835\text{S}_{000,\text{Na}} + 5.1073\text{S}_{100,\text{Na}} + 8.0311\text{S}_{200,\text{Na}} \\ &+ 10.9549\text{S}_{300,\text{Na}} - 3.3052\text{S}_{010,\text{Na}} - 0.3814\text{S}_{110,\text{Na}} + 2.5424\text{S}_{210,\text{Na}} + 5.4662\text{S}_{310,\text{Na}} \\ &- 3.2827\text{S}_{001,\text{Na}} - 0.3589\text{S}_{101,\text{Na}} + 2.5649\text{S}_{201,\text{Na}} + 5.4887\text{S}_{301,\text{Na}} - 8.7714\text{S}_{011,\text{Na}} \\ &- 5.8476\text{S}_{111,\text{Na}} - 2.9238\text{S}_{211,\text{Na}} - 1.5253\text{S}_{000,\text{LCC}} - 4.5742\text{S}_{010,\text{LCC}} - 0.2808\text{S}_{020,\text{LCC}} \\ &+ 2.7555\text{S}_{100,\text{LCC}} - 0.2933\text{S}_{110,\text{LCC}} + 4\text{S}_{120,\text{LCC}} - 5.5253\text{S}_{001,\text{LCC}} - 8.5742\text{S}_{011,\text{LCC}} \\ &- 4.2808\text{S}_{021,\text{LCC}} - 1.2445\text{S}_{101,\text{LCC}} - 4.2933\text{S}_{111,\text{LCC}} + \text{P2}_{\text{NaK}} + \text{P3}_{\text{NaK}} + \text{P4}_{\text{NaK}} \\ &- 0.9450\text{P6}_{\text{NaK}} - 0.9450\text{P7}_{\text{NaK}} - 0.9450\text{P8}_{\text{NaK}} - \text{P1}_{\text{NCX}} + 2\text{P2}_{\text{NCX}}\end{aligned} \tag{S67}$$

References

1. Kennedy J, Eberhart R. 1995 Particle swarm optimization. In *IEEE International Conference on Neural Networks, 1995. Proceedings* vol. 4 pp. 1942–1948 vol.4.
2. Gawthrop PJ, Siekmann I, Kameneva T, Saha S, Ibbotson MR, Crampin EJ. 2017 Bond graph modelling of chemoelectrical energy transduction. *IET Syst. Biol.* **11**, 127–138. doi:10.1049/iet-syb.2017.0006.
3. Luo CH, Rudy Y. 1994 A dynamic model of the cardiac ventricular action potential. I. Simulations of ionic currents and concentration changes.. *Circ. Res.* **74**, 1071–1096. doi:10.1161/01.RES.74.6.1071.
4. Rasmusson RL, Clark JW, Giles WR, Robinson K, Clark RB, Shibata EF, Campbell DL. 1990 A mathematical model of electrophysiological activity in a bullfrog atrial cell. *Am. J. Physiol-heart. C.* **259**, H370–H389.
5. Smith NP, Crampin EJ. 2004 Development of models of active ion transport for whole-cell modelling: cardiac sodium–potassium pump as a case study. *Prog. Biophys. Mol. Biol.* **85**, 387–405. doi:10.1016/j.pbiomolbio.2004.01.010.
6. Pan M, Gawthrop PJ, Cursons J, Tran K, Crampin EJ. 2017 The cardiac Na^+/K^+ ATPase: An updated, thermodynamically consistent model. *arXiv:1711.00989 [q-bio]*.
7. Giladi M, Shor R, Lisnyansky M, Khananshvili D. 2016 Structure-Functional Basis of Ion Transport in Sodium–Calcium Exchanger (NCX) Proteins. *Int. J. Mol. Sci.* **17**. doi:10.3390/ijms17111949.
8. Hilgemann DW, Matsuoka S, Nagel GA, Collins A. 1992 Steady-state and dynamic properties of cardiac sodium-calcium exchange. Sodium-dependent inactivation.. *The Journal of General Physiology* **100**, 905–932. doi:10.1085/jgp.100.6.905.
9. Kimura J, Miyamae S, Noma A. 1987 Identification of sodium-calcium exchange current in single ventricular cells of guinea-pig.. *The Journal of Physiology* **384**, 199–222. doi:10.1113/jphysiol.1987.sp016450.

10. Beuckelmann DJ, Wier WG. 1989 Sodium-calcium exchange in guinea-pig cardiac cells: exchange current and changes in intracellular Ca^{2+}.. *The Journal of Physiology* **414**, 499–520. doi:10.1113/jphysiol.1989.sp017700.
11. Gawthrop PJ, Cursons J, Crampin EJ. 2015 Hierarchical bond graph modelling of biochemical networks. *Proc. R. Soc. A* **471**, 20150642. doi:10.1098/rspa.2015.0642.
12. Reuter H. 1984 Ion channels in cardiac cell membranes. *Annu. Rev. Physiol.* **46**, 473–484.
13. Sakmann B, Trube G. 1984 Conductance properties of single inwardly rectifying potassium channels in ventricular cells from guinea-pig heart.. *J Physiol* **347**, 641–657.
14. Shibasaki T. 1987 Conductance and kinetics of delayed rectifier potassium channels in nodal cells of the rabbit heart.. *The Journal of Physiology* **387**, 227.
15. Yue L, Feng J, Li GR, Nattel S. 1996 Characterization of an ultrarapid delayed rectifier potassium channel involved in canine atrial repolarization.. *J Physiol* **496**, 647–662.
16. Hinch R, Greenstein JL, Tanskanen AJ, Xu L, Winslow RL. 2004 A Simplified Local Control Model of Calcium-Induced Calcium Release in Cardiac Ventricular Myocytes. *Biophys. J.* **87**, 3723–3736. doi:10.1529/biophysj.104.049973.